JOURNAL OF PROPULSION AND POWER
Vol. 22, No. 5, September–October 2006

Characteristics of Dual Transverse Injection in Scramjet Combustor, Part 1: Mixing

Sang-Hyeon Lee*
University of Ulsan, Ulsan 680-749, Republic of Korea

DOI: 10.2514/1.14180

The mixing characteristics of a dual transverse injection system in a scramjet combustor were studied with numerical methods. The effects of the jet-to-cross-flow momentum flux ratio and the distance between injectors on mixing characteristics were investigated. Three-dimensional Navier–Stokes equations, including the k–ω SST turbulence model, were solved with the finite volume method adopting the upwind method of Edwards' low diffusion flux splitting scheme. It is shown that the mixing characteristics of a dual transverse injection system are very different from those of a single injection system. The rear injection flow is strongly influenced by blockage effects due to the momentum flux of the front injection flow and thus has higher expansion and penetration than the front injection flow. The dual injection system has a higher mixing rate and a higher penetration but have more losses of stagnation pressure than the single injection system. It is also shown that there is an optimal distance between injectors for mixing characteristics and that the optimal distance increased as the jet-to-cross-flow momentum flux ratio increased.

Nomenclature

D	=	diameter of single injection hole
J	=	jet-to-cross-flow momentum flux ratio
k	=	turbulent kinetic energy
L	=	half distance between injectors
M	=	Mach number
N_s	=	number of chemical species
P_o	=	average stagnation pressure
p	=	static pressure
r_{H_2}	=	effective radius of hydrogen
T	=	temperature
Y	=	mass-fraction
Z_{H_2}	=	penetration distance of hydrogen fuel jet
Γ	=	circulation normalized by Du_∞
μ, ν	=	viscosity and dynamic viscosity
ρ	=	density
σ_{H_2}	=	standard deviation of hydrogen distribution
χ_s	=	mass diffusivity of s species
ω	=	turbulent dissipation variable

Subscript

f	=	fuel jet
o	=	stagnation
s	=	chemical species
∞	=	inflow condition

Superscript

d	=	diffusion

Introduction

ONE of the critical issues for the design of a scramjet (supersonic combustion ramjet) combustor is the mixing problem due to the short residence time of airflow within a scramjet combustor. The residence time of airflow in a scramjet engine is only about a millisecond for typical flight conditions. Therefore, rapid and efficient fuel–air mixing is necessary, while the stagnation pressure loss and the heat loads on combustor walls must be minimized [1–5]. A conventional and reliable method of fuel injection for a scramjet engine is a transverse injection into the supersonic airflow, because transverse injection provides rapid fuel–air mixing and high jet penetration into the supersonic airflow. Transverse injection into a supersonic crossflow has been the subject of many experimental and computational studies including mixing, combustion, ignition and measuring technologies [6–15].

Recently, there have been many research activities [16–19] to investigate the mixing and combustion characteristics of multiple transverse injection systems or aerodynamic ramp injection systems. These experimental and computational studies have reported that an aerodynamic ramp injection system have better mixing characteristics than a single transverse injection system and would be a realistic method for fuel–air mixing in a scramjet combustor. The flow field of a multiple transverse injection system in a supersonic airflow is even more complex than that of a single transverse injection system due to the interactions among the injection flows. Complications of an efficient injection system setup also arise due to many other parameters, including positioning of the each injector, distributions of mass flow rate and momentum flux, injection angle, and combination of injection angles. Therefore, it is very difficult to analyze the mixing and combustion characteristics of a multiple transverse injection system. Thus, it is necessary to investigate the mixing characteristics of a simplified model of a multiple transverse

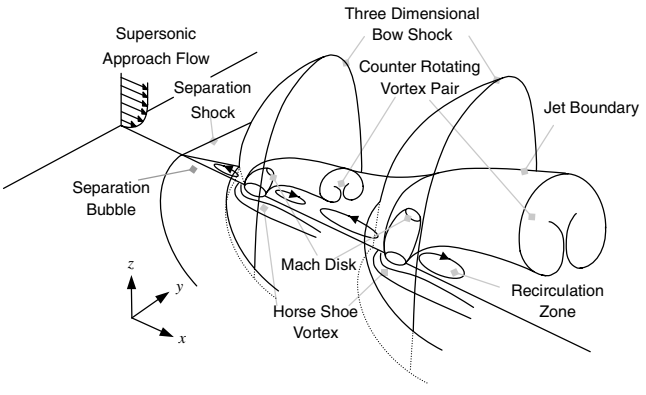

Fig. 1 Schematic view of mean flowfield of dual transverse injection.

Received 25 October 2004; revision received 12 January 2006; accepted for publication 21 January 2006.

*Associate Professor, Department of Aerospace Engineering; lsh@mail.ulsan.ac.kr. Member AIAA.

injection system at the beginning stage. The present study chose a dual transverse injection system as a basic model for multiple transverse injection systems in which the injectors are located in a line.

The flow field of dual transverse injection into a supersonic crossflow is very complex due to various shock structures and vortical flows around injection flows. Figure 1 shows the schematic of the dual transverse injection. There are many shock waves: three-dimensional bow shocks formed ahead of the front jet and ahead of the rear jet, a separation shock generated by the interaction between the front bow shock and boundary layer, and Mach discs. A distinctive feature of the dual injection is that the Mach disc of the rear jet is located at higher position from the wall and is larger than the Mach disc of the front jet. The front jet blocks the supersonic air flow blowing towards the rear jet. This blocking of air flow would have significant influences on the mixing process. There are also many vortical flow features. Vortex pairs formed along the jet flows, horse shoe vortices, separation bubble and recirculating wake flows. The evolution of the vortex pair is a very complex process involving three-dimensional tilting and folding. Streamwise vortices roll up injection flows and thus accelerate the fuel–air mixing in supersonic flow fields [7,8,14,15,20].

The main objective of the present study is to analyze the interactions between jet flows and to investigate the influences of these interactions on the mixing characteristics of a dual transverse injection system. The influences of the airflow blocking and the evolution of streamwise vortices on mixing characteristics are presented in detail. The most important parameters affecting the blockage effects and the evolution process of streamwise vortices are the distance between injectors and the jet-to-cross-flow momentum flux ratio. There would be an optimal distance between injectors for the mixing characteristics, and the optimal distance would change according to the jet-to-cross-flow momentum flux ratio. Thus, the existence of optimal condition and the changes of optimal condition due to key parameters are discussed in detail.

The mixing parameters considered in the present study are mixing rate, penetration distance, and stagnation pressure loss. Mixing rate is one of the most important parameters, because the burning rate in a scramjet combustor is mainly determined by the mixing rate. The penetration of injectant is also an important parameter, because the fuel should be far enough away from the combustor wall to enhance fuel–air mixing and to avoid wall heating in a scramjet combustor. An excessive loss of stagnation pressure should be avoided because a loss of stagnation pressure results in a loss of thrust.

Calculation Methods

Governing Equations

Three-dimensional Navier–Stokes equations are solved to obtain mean flow fields and the k–ω SST turbulence model [21–23] is solved to obtain turbulent viscosity. These governing equations are expressed in vector form as follows:

$$\frac{\partial Q}{\partial t}+\frac{\partial E_j}{\partial x_j}=\frac{\partial E_{vj}}{\partial x_j}+S_T \tag{1a}$$

$$Q=\begin{bmatrix}\rho_s\\ \rho u_i\\ \rho e_o\\ \rho k\\ \rho\omega\end{bmatrix},\qquad E_j=\begin{bmatrix}\rho_s u_j\\ \rho u_i u_j+\delta_{ij}\\ \rho h_o u_j\\ \rho k u_j\\ \rho\omega u_j\end{bmatrix},$$
$$E_{vj}=\begin{bmatrix}\rho_s u_{sj}^d\\ \tau_{ij}\\ \tau_{jk}u_k-q_j\\ (\mu_L+\sigma^*\mu_T)\frac{\partial k}{\partial x_j}\\ (\mu_L+\sigma\mu_T)\frac{\partial\omega}{\partial x_j}\end{bmatrix},\quad\text{and}\quad S_T=\begin{bmatrix}0\\0\\0\\P_k\\P_\omega\end{bmatrix} \tag{1b}$$

Q is the solution vector, E_j is the convection vector in the j direction, and E_{vj} is the viscous vector in the j direction, respectively. S_T is the turbulent source vector. P_k and P_ω are the source terms of the variables k and ω, respectively. The definition of turbulent viscosity and the model coefficients are the same as those of Menter's k–ω SST turbulence model. For details, refer to Menter [21]. A model for the dilatation–dissipation term suggested by Wilcox [23] is included to predict the compressibility effects.

Three chemical species (nitrogen, oxygen, and hydrogen) are considered for calculating the mixing process. These species are assumed to be ideal gases. The thermodynamic state equation for ideal gas is expressed as

$$p=\rho T\sum_s^{N_S}\frac{Y_s}{W_s},\quad\text{where }\rho=\sum_{s=1}^{N_S}\rho_s \tag{2}$$

The symbol W_s denotes the molecular weight of species s. The diffusion velocity of each species is determined by Fick's law as

$$Y_s u_{sj}^d=-\chi_s\frac{\partial Y_s}{\partial x_j} \tag{3}$$

where the coefficient χ_s is the diffusivity of species s.

The formula and data of viscosity, thermal conductivity and binary diffusivity were taken from Reid et al. [24], where the intermolecular potential function was the Lennard–Jones 12-6 potential. The viscosity of a pure gas was obtained from the Chapman–Enskog equation, and the viscosity of a gas mixture was calculated using the Wilke law. The thermal conductivity of a pure gas is obtained from the Eucken method and the thermal conductivity of the gas mixture was calculated by the Wassiljewa equation modified by Mason and Saxena. The diffusivity of a binary gas mixture is determined by the Chapman–Enskog equation, and the diffusivity of a gas in the gas mixture is determined by the Blanc's law. Turbulent diffusivity and turbulent conductivity are obtained from the turbulent viscosity. The turbulent Prandtl number and turbulent Schmidt number were both 0.9.

A finite volume method is used to discretize the governing equations. The inviscid fluxes were discretized in third order spatial accuracy according to the low diffusion flux splitting scheme of Edwards [25]. The diffusion vectors are discretized with second order central difference scheme. Time integration was performed using the lower upper symmetric Gauss Seidel scheme [26].

Geometry of Models and Grid Systems

In the present study, two kinds of injector models are considered. Model S is the canonical model with an injection hole located at the origin of the coordinate system. Model DN is a model with two injectors where the number N stands for the half distance between the two injectors. The two injectors are symmetrically located with respect to the origin. For instance, in model D3, the front injector is located at $x=-3D$ and the rear injector is located at $x=3D$, thus the distance between injectors is $6D$. In the present study, six cases of dual injection systems are considered: D1, D2, D3, D4, D5, and D7.

Figure 2 shows the geometries and grid systems near the injection hole of the model combustors. The diameter of the circular injection hole in the single injection system (D) is 3.18 mm (as same as that of Gruber's experiment [15]). The length of the combustor model is $(43+N)\times D$ ($8D$ before the front injection hole and $35D$ after the origin), the width is $10D$, and the height is $12D$. The round jet is made with a numerical technique as follows:

$$w_{\text{wall}}=f(r)a_f,\qquad f(r)=\begin{cases}1, & r\le R-\delta\\ \sqrt{R-r}/\sqrt{\delta}, & R-\delta\le r\le R\\ 0, & r>R\end{cases} \tag{4}$$

The symbol w_{wall} denotes the vertical velocity of the fuel jet through the injection hole, the symbol a_f denotes the sonic speed of the fuel jet, the symbol r denotes the distance from the center of the injection hole, the symbol R denotes the radius of the injection hole and the symbol δ is the thickness of the boundary layer. The boundary

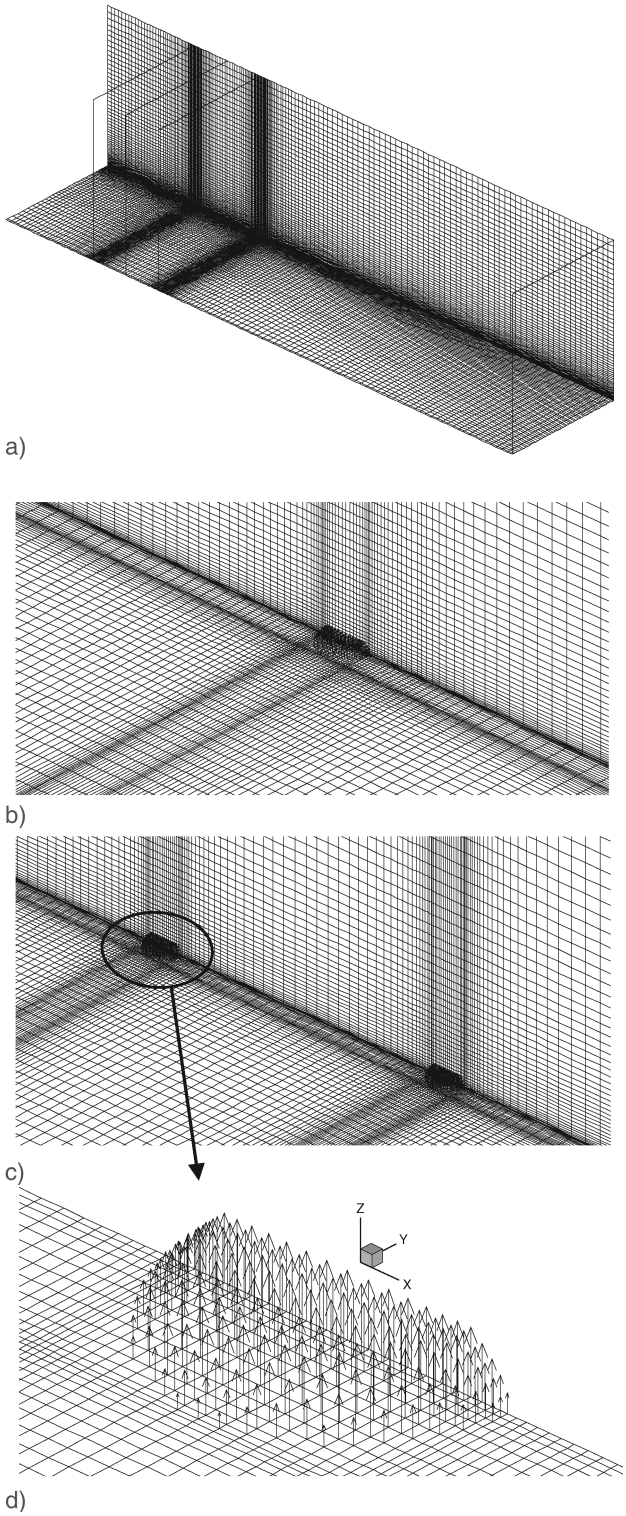

Fig. 2 Grid systems: a) whole grids of model D3; b) grids near injection hole in model S; c) grids near injection hole in model D3; and d) numerical formation of round jet flow in Cartesian grid system.

thickness is $0.2D$ as recommended in Lee and Mitani [20]. The grid points are clustered towards the boundary of the injection hole in order to make the cross-sectional shape of the jet a circular one as illustrated in Fig. 2d.

The number of grid points (N_G) of model S is $604,500 (= 155[x] \times 60[y] \times 65[z])$. The number of grid points of the y–z plane of a model DN is same as that of model S. The number of grid points in the x direction of a model DN is determined considering the model number N or the distance between injectors: 180 for model D1 ($N_G = 702,000$), 189 for model D2 ($N_G = 737,100$), 198 for model D3 ($N_G = 772,200$), 203 for model D4 ($N_G = 791,700$), 205 for model D5 ($N_G = 799,500$), 209 for model D7 ($N_G = 815,100$). Eighteen grid points are placed within each injection hole in the x direction and 11 grid points are placed within each injection hole in the y direction, also grid points near an injection hole were clustered to maintain the smooth distribution of grid points. The grid points are clustered towards the wall to ensure that the first grid point away from the wall is placed within the viscous sublayer ($y^+ = u_\tau y/\nu < 5$).

Flow Conditions and Boundary Conditions

The airflow conditions at the infinite far fields are those of Mach 6 flight at 35 km altitude in the standard atmosphere, where the static pressure and temperature are 559 Pa and 237 K, respectively. The inlet conditions are calculated with the isentropic relations considering that the flow at the infinite far field is decelerated down to Mach 2 at the inlet of a scramjet combustor. The static pressure and temperature of the airflow at the inlet position are 146.6 kPa and 1081 K, respectively. The fuel is hydrogen. The fuel is vertically injected into the airflow at sonic condition. J is one of the most important parameters determining mixing characteristics. J is defined as follows:

$$J \equiv \frac{(\rho V^2)_f}{(\rho V^2)_\infty} = \frac{(\gamma p M^2)_f}{(\gamma p M^2)_\infty} \tag{5}$$

In the present work, a parametric study was conducted with a variation of the magnitude of J from 1.0 to 2.0. The stagnation temperature of the hydrogen fuel is 600 K, and the static pressure. The static pressure of the jet is determined by Eq. (7). Then, the temperature and density are determined by the isentropic relations. The flow conditions of the front injection and the rear injection are the same to each other. The total mass flow rate of a dual injection system is the same as the mass flow rate of a single injection system. The flow rate is controlled with the area of the injection hole, thus the diameters of the dual injection holes are the same and are determined as follows:

$$D_{\text{front}} = D_{\text{rear}} = \frac{D}{\sqrt{2}} \tag{6}$$

Calculations are conducted on the half-domain with respect to the symmetric plane of the injection hole in order to reduce computation time. The top surface and right surface of the computational domain are treated as open boundaries. The solid wall is treated as a constant-temperature no-slip wall. The wall temperature is fixed to the inflow air temperature. The boundary conditions of the turbulence model on solid walls are as follows:

$$k = 0, \qquad \omega = 10\frac{6\nu}{\beta_1^*(\Delta y_1)^2} \tag{7}$$

where Δy_1 is the distance of the first grid point from wall. The turbulent viscosities of the inflow and the jet flow are both 0.01 times the laminar viscosity of the inflow air as recommended by Menter [21].

Code Validation

The computational code used in the present study is the same used in the previous study [20]. In that work the validation study was conducted and discussed in detail. The calculation results with the present code are compared with the experimental results of Gruber et al. [15] The wall pressure along the center axis ($y = 0$) and the wall pressure around the injection hole are calculated with the present computational code. Also, a grid independence study was performed with two additional grid resolutions. The number of grid points of the second grid system is 46% of the primary grid system, while the number of grid points of the third grid system is 180% of the primary grid system. Even the calculation on the second grid system with the smallest number of grid points showed almost the same results as the

experimental results of Gruber et al. except for a small region in front of the injection hole; the largest difference is about 9% of the experimental datum. The calculation on third grid system showed almost same results as those on the primary grid system; the largest difference is about 3% of the experimental datum. Thus, it can be stated that the present computational code is a credible one and the present grid system have enough number of grid points. For details, refer to Lee and Mitani [20].

Results

Overall Mixing Characteristics

To compare the overall trends of the mixing characteristics between the dual injection systems and the single injection system, the distributions of injectant mass fraction are plotted in Fig. 3. Figures 3a and 3b compare the mixing processes between model S and model D4 when the magnitude of J is 1.0, while Figs. 3c and 3d compare the mixing processes between model S and model D4 when the values of J is 2.0.

The case with a higher magnitude of J has a higher penetration of injectant into the airflow and a higher maximum mass fraction of hydrogen at a cross section plane. Considering that the case with a higher mixing rate have a lower maximum mass fraction of fuel [20,27–29], the case with a higher magnitude of J has slower fuel–air mixing. The penetration in model D4 is higher than in model S and the mixing rate in model D4 is higher than in model S when the values of J are the same. What is the reason of the mixing augmentation of the dual injection system with respect to that of the single injection system? It is noticed that the rear injection flow in a dual injection system has a higher flow expansion than the front injection flow and even higher than the single injection flow. This might have been the result of the "blockage effect" in which the front injection flow blocks the airflow towards the rear injection flow leading to a reduction of the momentum of the airflow. Thus the effective jet-to-crossflow momentum flux ratio of the rear injection flow increased, which assists the rear injection flow stronger expansion.

To investigate the blockage effects in detail, the pressure fields near the injection holes in the x–z plane are plotted in Fig. 4. The figures in the left column show the pressure fields when the magnitude of J is 1.0, while the figures in the right column show the pressure fields when the magnitude of J is 2.0. The case with a higher magnitude of J show stronger shock waves and thus higher pressure jumps due to stronger interactions between airflow and injection flow. In a general sense, the strengths of the shock waves ahead of the rear injection flows are weaker than near the front injection flows, which implied that the front injection flows blocked the airflow ahead of the injection flows and assisted the rear injection flows to expand more strongly. On the other hand, the structures and strengths of the shock waves near the rear injection flow are closely related to the distance between injectors, while the structure and strength of the shock waves near the front injection flows are maintained regardless of the distance between injectors. The strength of the shock waves over the rear injection flows decreased but the strength of the shock

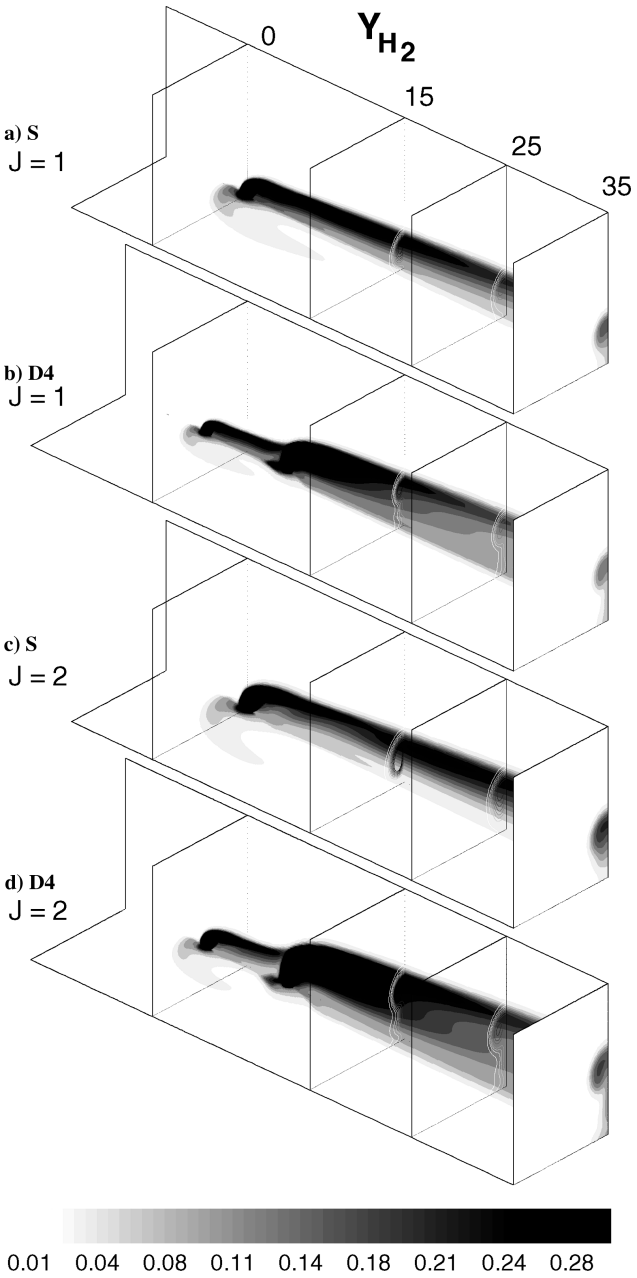

Fig. 3 Comparisons of mixing process between single injection systems and dual injection systems. Drawn quantity is hydrogen mass-fraction. The values higher than 0.3 are cut off.

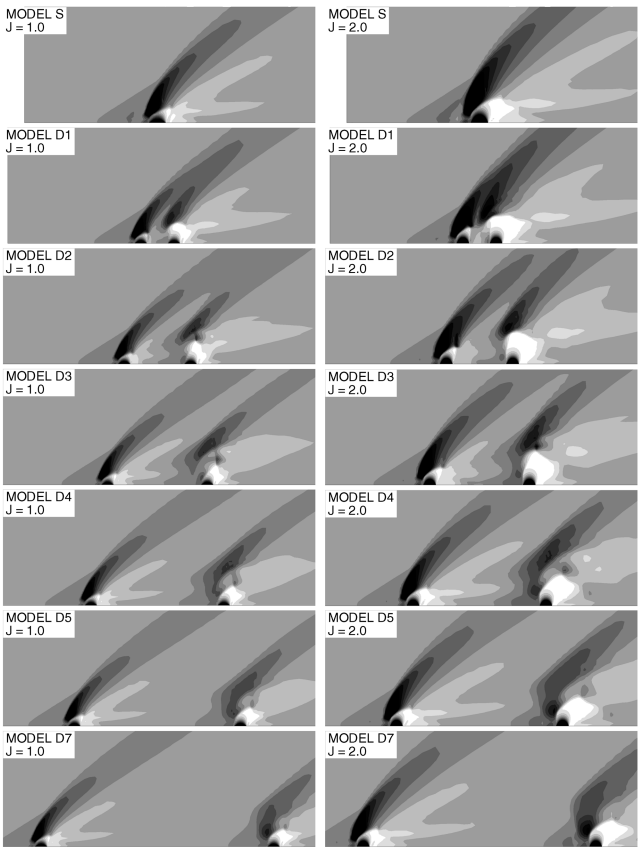

Fig. 4 Comparison of pressure fields near injection holes. The darker region has higher pressure. The highest pressure is $6.7p_\infty$.

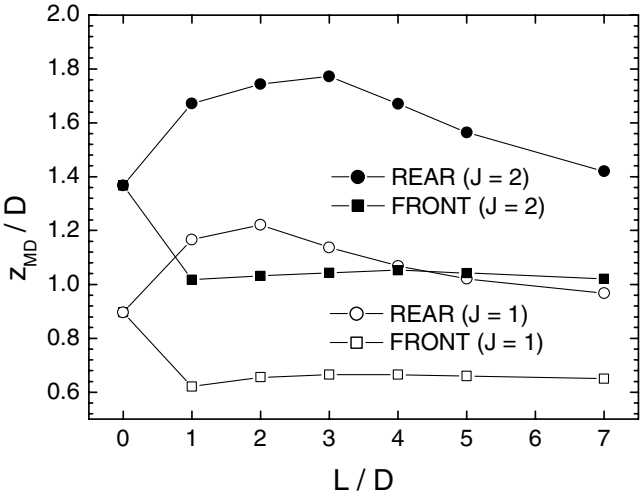

Fig. 5 Variations of height of Mach disc due to distance between injectors.

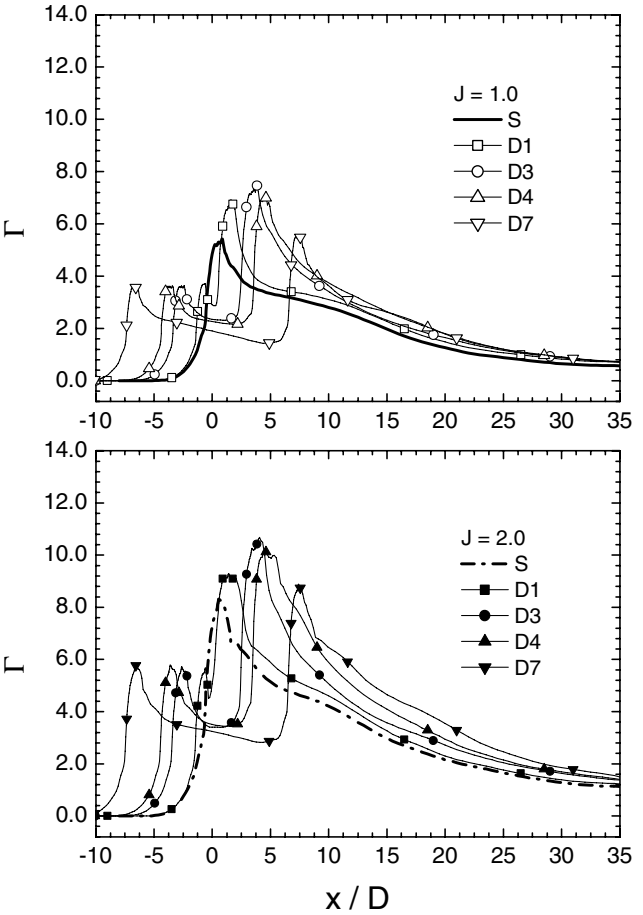

Fig. 6 Comparison of circulation normalized by diameter of injection hole and velocity of inflow air.

waves near the front of the rear injection flows increased as the distance between injectors increased. These two contrary variations of shock structures suggested that there would be an optimal distance between injectors for blockage effects.

It is well known that a significant parameter determining mixing characteristics is the height of the Mach disc [6–8]. Figure 5 shows the variations of the height of the Mach disc due to the magnitude of J and due to the distance between injectors. The case with a higher magnitude of J shows a higher height of the Mach disc and a larger difference of the height of the Mach disc between the front and rear injection flows. The height of the Mach disc of the rear injection flow is strongly related with the distance between injectors, while the height of the Mach disc of the front injection flows is maintained regardless of the distance between injectors. The Mach disc height of the front injection flow in the dual injection system is smaller than that of the single injection system because the diameter of injection hole of the dual injection system is smaller than that of the single injection system as mentioned in Eq. (6). The heights of the Mach discs of the rear injection flows are higher than those of the front injection flows, which is due to the blockage effects previously mentioned. Model D2 shows the highest height of the Mach disc of the rear injection flows when the magnitude of J is 1.0, while model D3 shows the highest height of the Mach disc of the rear injection flows when the magnitude of J is 2.0. This suggests that the blockage effects increased and thus the optimal distance between injectors for mixing characteristics increased with increasing J.

Streamwise Vorticities

It is well known that streamwise vorticity has a great influence on the mixing process in high-speed flows [27–31]. To represent the effects of streamwise vorticity as a scalar in a y–z plane the circulation is considered. The definition of the normalized circulation is expressed in the following form:

$$\Gamma(x) = \frac{1}{Du_\infty} \oint \int \left| \frac{\partial v}{\partial z} - \frac{\partial w}{\partial y} \right| \mathrm{d}y\, \mathrm{d}z \tag{8}$$

The histories of circulation of all models are compared in Fig. 6. The strength of circulation is closely related to the magnitude of J (jet-to-crossflow momentum flux ratio). The case with a higher magnitude of J has a stronger streamwise vorticity, which might have been due to the stronger flow deflections by the shock waves and expansion waves. Another possible reason is that the case with a higher magnitude of J has a higher density and thus produced stronger baroclinic vorticity [27–29]. There are two jumps of circulation in a dual injection system at the front and the rear injection holes, while there is a single jump of circulation in the single injection system. The first peak of the circulation in the dual injection system is smaller than the peak of the single injection system because the diameter of injection hole of the dual injection system is smaller than that of the single injection system. The circulation of a dual injection system is higher than of the single injection system, which suggested that a dual injection system would have better mixing characteristics than the single injection system. The strengths of the first jumps in dual injection systems are consistent from case to case. The strengths of the second jumps increased as the distance between injectors increased until a critical distance, and then decreased after that critical distance. This suggests that there is an optimal distance between injectors for streamwise vorticity and thus mixing characteristics.

Mixing Rates

The mixing rate is one of the most important parameters of mixing characteristics because the combustion process in supersonic flow fields strongly depends on the mixing process. Even though there are many definitions of mixing rate, in the present study, the definition in the articles [20,27–29] is used for the comparison with the previous experimental and numerical results. This definition of mixing rate is based on the decay rate of the maximum mass-fraction of fuel. Figure 7 shows the comparison of mixing rates. The decay rate of the maximum mass-fraction of the injectant in an injection system is drastically changed at the near fields but is almost linear on the log–log scale at the far fields. This is due to the fact that the mixing process largely depended on flow convection at the near fields but on mass diffusion at the far fields. Therefore, there is a transition from a convection-dominated regime to a diffusion-dominated regime because there are no flow-acceleration mechanisms at the far field [27,28].

The mixing rates of the dual injection systems are higher regardless of the magnitude of J compared with the single injection

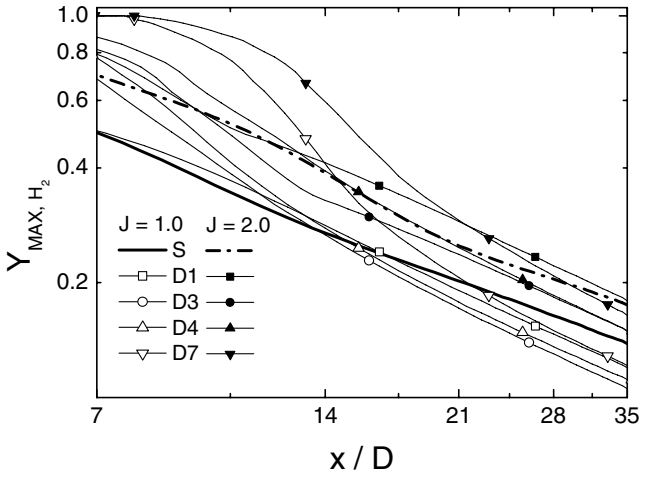

Fig. 7 Comparison of mixing rate expressed by decay rate of maximum mass-fraction of injectant (plotted on log–log scale).

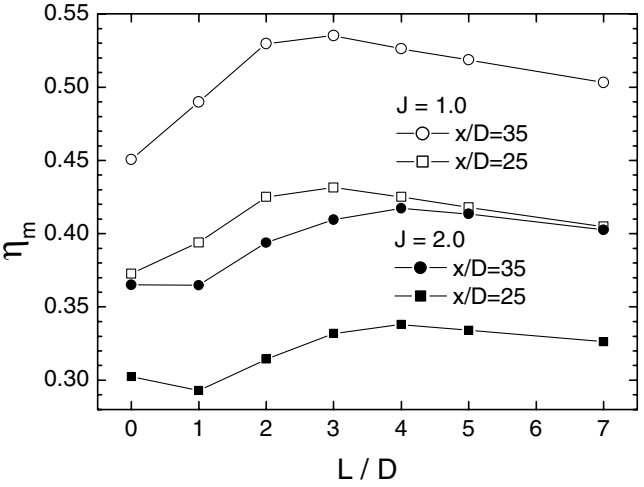

Fig. 8 Variations of mixing efficiencies due to distance between injectors at $x/D = 25$ and $x/D = 35$.

system due to higher circulations. As mentioned in the previous articles [20,27–31], streamwise vorticity, or vortex pair, produces a large convection flow in the plane perpendicular to the streamwise direction and promotes fuel–air mixing and thus a higher mixing rate largely depended on a higher streamwise vorticity. Mixing rates are closely related to the magnitude of J. The case with a lower magnitude of J shows a faster mixing than with a higher magnitude of J. This is due to the fact that a smaller magnitude of J has a weaker inertia of jet flow and thus the airflow could more easily disturb or stir the jet flow with a lower magnitude of J. Also, the mixing rate of a dual injection system depended on the distance between injectors. Model D3 show the fastest mixing when the magnitude of J is 1.0, while model D4 show the fastest mixing when the magnitude of J is 2.0. This shows the same trend in the analyses of the circulations. These facts suggested that the there is an optimal distance for mixing rates and that this distance increased as the magnitude of J increased.

The concept of mixing efficiency [11,19] is adopted to quantify mixing capabilities. Mixing efficiency is defined as follows:

$$\eta_m(x) = \oint\int Y_{H_2}\rho u \,\mathrm{d}y\,\mathrm{d}z \Big/ \oint\int Y^r_{H_2}\rho u \,\mathrm{d}y\,\mathrm{d}z \tag{9a}$$

$$Y^r_{H_2} = \begin{cases} Y_{H_2}, & Y_{H_2} \le Y^{\text{stoic}}_{H_2} \\ \left(\frac{1-Y_{H_2}}{1-Y^{\text{stoic}}_{H_2}}\right) Y^{\text{stoic}}_{H_2}, & Y_{H_2} > Y^{\text{stoic}}_{H_2} \end{cases} \tag{9b}$$

where $Y^{\text{stoic}}_{H_2}$ stands for the stoichiometric mass fraction for a hydrogen–air mixture. Figure 8 shows the variation of mixing efficiency due to the magnitude of J and due to the distance between injectors downstream at $x/D = 25$ and $x/D = 35$. The mixing efficiency of a dual injection system is higher than of the single injection system, which is consistent with the results of Jacobsen et al. [19] The case with a higher magnitude of J have a lower mixing efficiency due to a higher inertia as mentioned above. The mixing efficiencies at $x/D = 35$ are higher than at $x/D = 25$, which implied that mixing progressed as the flows went downstream. However, the variation pattern of mixing efficiency due to the distance between injectors is well maintained. There is a strong relationship between mixing efficiency and the distance between injectors. Model D3 have the highest mixing efficiency when the magnitude of J is 1.0, while model D4 have the highest mixing efficiency when the magnitude of J is 2.0. These facts suggested that the there is an optimal distance for mixing efficiency and that the optimal distance increased as the magnitude of J increased.

The concepts of the effective radius of hydrogen fuel and the standard deviation of effective radius are introduced in order to estimate the relationship between mixing rates and hydrogen flame structures. The case with a larger effective radius would have a wider distribution of hydrogen, while the case with a larger standard deviation would have a more complex structure or a wider contact surface between the hydrogen fuel and air. The definitions of the effective radius of hydrogen fuel and the standard deviation are as follows:

$$r_{H_2}(x) = \oint\int \rho_{H_2}|\mathbf{r} - \mathbf{c}| \,\mathrm{d}y\,\mathrm{d}z \Big/ \oint\int \rho_{H_2} \,\mathrm{d}y\,\mathrm{d}z \tag{10a}$$

$$\sigma^2_{H_2}(x) = \oint\int \rho_{H_2}(|\mathbf{r} - \mathbf{c}| - r_{H_2})^2 \,\mathrm{d}y\,\mathrm{d}z \Big/ \oint\int \rho_{H_2} \,\mathrm{d}y\,\mathrm{d}z \tag{10b}$$

The vectors $\mathbf{r}$ and $\mathbf{c}$ are the position vector at a location in a y–z plane and the position vector of the mass center of hydrogen, respectively. Figure 9 shows the comparison of the effective radii of hydrogen flames in a y–z plane. The first peak of the effective radius in the dual injection system is smaller than the peak of the single injection system because the diameter of injection hole of the dual injection system is smaller than that of the single injection system. The effective radii are related to the magnitude of J but the degree of variation is relatively small considering that the case with twice the magnitude of J has twice the mass flow rate. The case with the J magnitude of 2.0 has a slightly larger effective radius and a slightly larger standard deviation than with the J magnitude of 1.0. This meant that the relative mixing rate decreased as the magnitude of J increased, which is consistent with the analyses of mixing rate and mixing efficiency mentioned in the above paragraphs. The effective radius is also strongly related to the distance between injectors. Model D3 have the largest effective radius of hydrogen fuel when the magnitude of J is 1.0, while model D4 have the largest effective radius of hydrogen fuel when the magnitude of J is 2.0. It should be noted that model D3 have a larger standard deviation than model D4 when the magnitude of J is 2.0, which implied that model D3 have a relatively wider contact surface between hydrogen and air and that the mixing capability of models D3 and D4 would be competitive with each other. These facts are consistent with the analyses of mixing rates and mixing efficiencies. Thus, the effective radius and its standard deviation are good indicators of mixing capabilities.

Penetrations

Injected fuel must penetrate high enough into the crossflow in order to minimize wall heating and to maximize combustion efficiency. Penetration distance is estimated with the center of mass of the fuel from the lower wall as follows:

$$Z_{H_2}(x) = \oint\int \rho_{H_2} z \,\mathrm{d}y\,\mathrm{d}z \Big/ \oint\int \rho_{H_2} \,\mathrm{d}y\,\mathrm{d}z \tag{11}$$

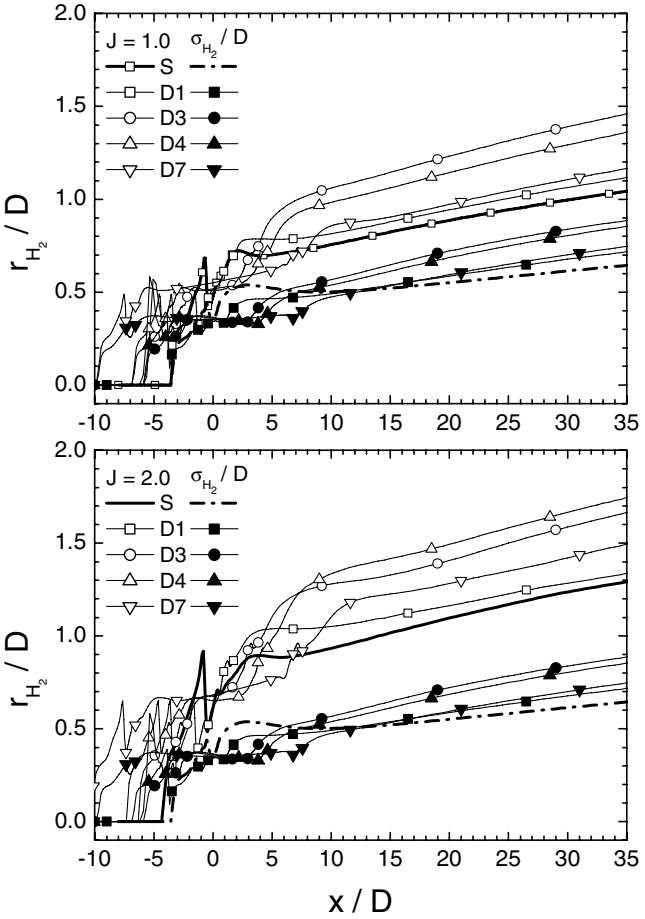

Fig. 9 Comparison of effective radii of fuel in y–z plane.

Figure 10 shows the comparison of penetrations of fuel into the airflow. The reference location $z = 0$ is the lower wall. In every case, the penetration distance increased rapidly immediately after the injection, but the increasing rate of penetration gradually decreased and finally became a constant at the far field.

The dual injection system has a higher penetration than that of the single injection system. The penetration distances are closely related to the magnitude of J. The case with a higher magnitude of J has a higher penetration than with a lower magnitude of J. This is due to the fact that the jet flow with a higher magnitude of J has a stronger inertia force relative to the crossflow than with a lower magnitude of J. There is a strong relationship between penetration and the distance between injectors. Model D3 have the highest penetration when the magnitude of J is 1.0, while model D4 have the highest penetration when the magnitude of J is 2.0. These facts suggested that the there is an optimal distance for penetration and that the optimal distance between injectors for penetration increased as the magnitude of J increased.

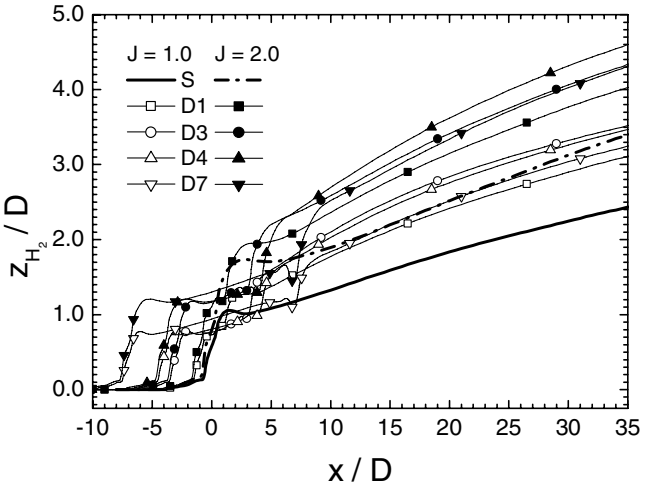

Fig. 10 Comparison of penetration distances.

Stagnation Pressure Losses

Generally, the mixing process produces a loss of stagnation pressure that results in a loss of thrust. Therefore, it is worth determining if there are additional losses of stagnation pressure due to mixing augmentation. The definition of average stagnation pressure in the y–z plane is expressed in the following form:

$$P_o(x) = \oint\int p_o \rho u \, \mathrm{d}y \, \mathrm{d}z \Big/ \oint\int \rho u \, \mathrm{d}y \, \mathrm{d}z \tag{12a}$$

$$\ell_n\left(\frac{p_o}{p}\right) = \frac{1}{R}\int_T^{T_o} \frac{c_p}{T}\,\mathrm{d}T$$

$$\text{where} \quad \int_0^{T_o} c_p \,\mathrm{d}T = \int_0^{T} c_p \,\mathrm{d}T + \tfrac{1}{2}(u^2 + v^2 + w^2) \tag{12b}$$

Figure 11 shows the histories of average stagnation pressures along the streamwise direction normalized by the stagnation pressures of the air inflow. All models show very similar histories of stagnation pressures; stagnation pressure slowly decreased in the region before the front injection holes but began to decrease very steeply in the region right after the injection holes. These rapid decreases of stagnation pressure are due to the shock waves in front of the jet flows and the fuel–air mixing.

Stagnation pressure losses are strongly related to the magnitude of J. The case of a higher magnitude of J shows more loss of stagnation pressure, which is due to stronger shock waves and stronger streamwise vorticity. In general, the dual injection systems have more losses of stagnation pressure than the single injection system. However, the increase of stagnation pressure losses in dual injection systems are not so great considering the mixing enhancement with respect to that of the single injection system. Model D1 shows less loss of stagnation pressure than of the single injection system and is an exceptional case. This can be explained with the analysis of mixing rates. Model D1 did not show a much higher mixing rate and penetration than the single injection system. The strengths of the shock waves in front of the injection flows are also much weaker than the single injection system. It should be noticed that model D7 shows more loss of stagnation pressure even though there are weak augmentations of mixing characteristics with respect to that of the single injection system. This may have been due to the fact that the rear injection flow suffered strong interaction between the airflow and the injection flow because of the weak blockage effects.

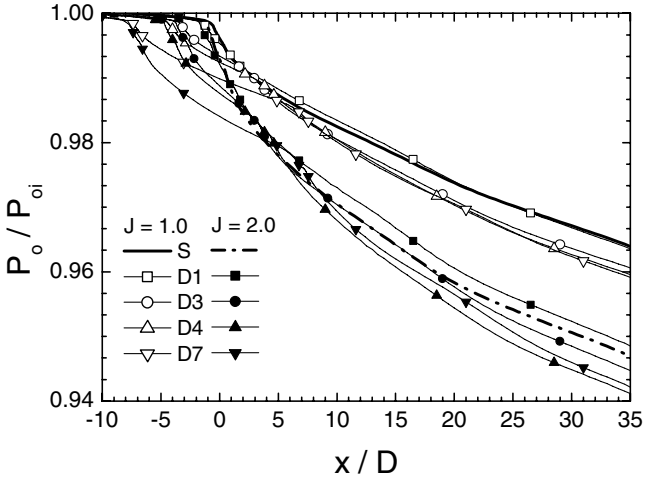

Fig. 11 Comparison of stagnation pressure normalized by stagnation pressure of inflow air.

Conclusion

In the present study, the mixing characteristics of a dual transverse injection system in a scramjet combustor were studied using numerical methods. Two kinds of parametric studies were conducted in order to investigate the variations of mixing characteristics due to J and due to the distance between injectors.

The mixing characteristics of a dual injection system are very different from those of a single injection system. The rear injection flow in a dual injection system is strongly influenced by the front injection flow. The rear injection flow has a higher expansion than the front injection flow due to the blockage effects, which resulted in better mixing characteristics: higher mixing rates and higher penetrations of fuel jet into the airflow. There is an optimal distance between injectors for blockage effects and the optimal distance increased as the magnitude of J increased.

The mixing characteristics are closely related to J. The case with a higher magnitude of J shows a higher penetration but a slower mixing. Also, the mixing characteristics are closely related to the distance between injectors in the dual injection systems. The mixing rates and penetrations increased as the distance between injectors increased until a critical distance but then decreased after that critical distance. Thus there existed an optimal distance between injectors for mixing characteristics, which coincided with the optimal distance for the blockage effects. The optimal distance between injectors for mixing characteristics increased as the magnitude of J increased.

Stagnation pressure losses are strongly related to the magnitude of J. The case of a higher magnitude of J shows more loss of stagnation pressure. A dual injection system suffered more loss of stagnation pressure with respect to the single injection system. The case with a higher mixing rate and a higher penetration suffered more loss of stagnation pressure. However, the increased losses of stagnation pressure of dual injection systems are not so great considering the mixing enhancement with respect to that of the single injection system.

Acknowledgments

This study was supported by the Research Program of University of Ulsan.

References

[1] Heiser, W. H., and Pratt, D. T., *Hypersonic Airbreathing Propulsion*, AIAA Education Series, AIAA, Washington, DC, 1994, pp. 79–80.

[2] Bogdanoff, D. W., "Advanced Injection and Mixing Techniques for Scramjet Combustors," *Journal of Propulsion and Power*, Vol. 10, No. 2, 1994, pp. 183–190.

[3] Bushnell, D. M., "Hypervelocity Scramjet Mixing Enhancement," *Journal of Propulsion and Power*, Vol. 11, No. 5, 1995, pp. 1088–1090.

[4] Riggins, D. W., McClinton, C. R., Rogers, R. C., and Bittner, R. D., "Investigation of Scramjet Injection Strategies for High Mach Number Flows," *Journal of Propulsion and Power*, Vol. 11, No. 3, 1995, pp. 409–418.

[5] Schetz, J. A., Billig, F. S., and Favin, S., "Modular Analysis of Scramjet Flowfields," *Journal of Propulsion and Power*, Vol. 5, No. 2, 1989, pp. 172–180.

[6] Zukoski, E. E., and Spaid, F. W., "Secondary Injection of Gases into a Supersonic Flow," *AIAA Journal*, Vol. 2, No. 10, October 1964, pp. 1689–1696.

[7] Schetz, J. A., Hawkins, P. F., and Lehman, H., "Penetration of Gaseous Jets Injected into a Supersonic Stream," *AIAA Journal*, Vol. 3, No. 11, 1966, pp. 1658–1665.

[8] Spaid, F. W., and Zukoski, E. E., "Further Experiments Concerning Secondary Injection of Gases into a Supersonic Flow," *AIAA Journal*, Vol. 4, No. 12, 1966, pp. 2216–2218.

[9] Billig, F. S., Orth, R. C., and Lasky, M., "A Unified Analysis of Gaseous Jet Penetration," *AIAA Journal*, Vol. 9, No. 6, 1971, pp. 1048–1058.

[10] Mao, M., Riggins, D. W., and McClinton, C. R., "Numerical Simulation of Transverse Fuel Injection," NASP CR 1089, 1990.

[11] Papamoschou, D., and Hubbard, D. G., "Visual Observations of Supersonic Transverse Jet," *Experiments in Fluids*, Vol. 14, No. 6, 1993, pp. 468–476.

[12] Wang, K. C., Smith, O. I., and Karagozian, A. R., "In Flight Imaging of Transverse Gas Jet Injected into Compressible Crossflows," *AIAA Journal*, Vol. 33, No. 12, 1995, pp. 2259–2263.

[13] Karagozian, A. R., Wang, K. C., Le, A. T., and Smith, O. I., "Transverse Gas Jet Injection behind a Rearward-Facing Step," *Journal of Propulsion and Power*, Vol. 12, No. 6, 1996, pp. 1129–1136.

[14] Everette, D. E., and Morris, M. J., "Wall Pressure Measurements for a Jet Injected Transversally into a Supersonic Crossflow," *Journal of Propulsion and Power*, Vol. 14, No. 6, 1998, pp. 861–868.

[15] Gruber, M. R., and Goss, L. P., "Surface Pressure Measurements in Supersonic Transverse Injection Flowfields," *Journal of Propulsion and Power*, Vol. 15. No. 5, 1999, pp. 633–641.

[16] Fuller, R. P., Wu, P. K., and Nejad, A. S., "Comparison of Physical and Aerodynamic Ramps as Fuel Injectors in Supersonic Flow," *Journal of Propulsion and Power*, Vol. 14. No. 2, 1998, pp. 134–145.

[17] Gallimore S. D., Jacobsen L. S., O'Brien W. F., and Schetz, J. A., "Operational Sensitivities of an Integrated Scramjet Ignition/Fuel-Injection System," *Journal of Propulsion and Power*, Vol. 19. No. 2, 2003, pp. 183–189.

[18] Jacobsen, S. D., Gallimore, S. D., Schetz, J. A., O'Brien, W. F., and Goss, L. P., "Improved Aerodynamic-Ramp Injector in Supersonic Flow," *Journal of Propulsion and Power*, Vol. 19. No. 4, 2003, pp. 663–673.

[19] Anderson, C. D., and Schetz, J. A., "Performance of an Aerodynamic Ramp Fuel Injector in a Scramjet Combustor," *Journal of Propulsion and Power*, Vol. 21. No. 2, 2005, pp. 371–374.

[20] Lee, S-H., and Mitani, T., "Mixing Augmentation of Transverse Injection in Scramjet Combustor," *Journal of Propulsion and Power*, Vol. 19. No. 1, 2003, pp. 115–124.

[21] Menter, F. R., "Two-Equation Eddy-Viscosity Turbulence Models for Engineering Applications," *AIAA Journal*, Vol. 32, No. 8, 1994, pp. 1598–1605.

[22] Menter, F. R., and Rumsey, C. L., "Assessment of Two Equation Turbulence Models for Transonic Flows," AIAA paper No. 94-2343, July 1994.

[23] Wilcox, D. C., *Turbulence Modeling for CFD*, DCW Industries, La Canada, CA, 1993, pp. 73–212.

[24] Reid, C. R., Prausnitz, J. M., and Poling, B. E., *The Properties of Gases and Liquids*, 4th ed., McGraw-Hill, New York, 1988.

[25] Edwards, J. R., "A Low-Diffusion Flux-Splitting Scheme for Navier–Stokes Calculations," *Computers and Fluids (1973-) / Computers & Fluids*, Vol. 26, No. 6, 1997, pp. 635–659.

[26] Yoon, S., and Jameson, A., "Lower-Upper Symmetric-Gauss-Seidel Method for the Euler and Navier–Stokes Equation," *AIAA Journal*, Vol. 26, No. 9, 1988, pp. 1025–1026.

[27] Lee, S-H., Jeung, I-S., and Yoon Y., "Computational Investigation of Shock-Enhanced Mixing and Combustion," *AIAA Journal*, Vol. 35, No. 12, 1997, pp. 1813–1820.

[28] Lee, S-H., Jeung, I-S., and Yoon Y., "Computational Investigation of Shock-Enhanced Mixing: Application to Circular Cross-Section Combustor," *AIAA Journal*, Vol. 36, No. 11, 1998, pp. 2055–2062.

[29] Waitz, I. A., Marble, F. E., and Zukoski, E. E., "Investigation of a Contoured Wall Injector for Hypervelocity Mixing Augmentation," *AIAA Journal*, Vol. 31, No. 6, 1993, pp. 1014–1021.

[30] Green, S. I., *Fluid Vorticity*, Kluwer Academic Publishers, Dordrecht, 1995, pp. 471–532.

[31] Ton, V. T., Karagozian, A. R., Marble, F. E., Osher, S. J., and Engquist, B. E., "Numerical Simulations of High-Speed Chemically Reacting Flow," *Theoretical and Computational Fluid Dynamics*, Vol. 6, No. 2, 1994, pp. 161–179.

J. Oefelein
Associate Editor